Composites Science and Technology 236 (2023) 109978

Contents lists available at ScienceDirect

Composites Science and Technology

journal homepage: www.elsevier.com/locate/compscitech

Current collector design strategies: The route to realising scale-up of structural power composites

M. Valkova [a,b], S. Nguyen [a,b], E. Senokos [c], S. Razavi [a,b], A.R.J. Kucernak [c], D.B. Anthony [c], M.S.P. Shaffer [b,c,d], E.S. Greenhalgh [a,b,*]

[a] Department of Aeronautics, Imperial College London, United Kingdom
[b] The Composites Centre, Imperial College London, United Kingdom
[c] Department of Chemistry, Imperial College London, United Kingdom
[d] Department of Materials, Imperial College London, United Kingdom

ARTICLE INFO

Keywords:
Multifunctional composites
Electrical properties
Computational modelling

ABSTRACT

Multifunctional structural power composites, which combine mechanical load-bearing and electrochemical energy storage, will transform electric vehicle design. This work focuses on structural supercapacitors, based on carbon aerogel-modified carbon fibre electrodes with copper current collectors. In common with many structural power embodiments, scale-up of these devices is currently limited by large internal resistances and the mass associated with current collection. There is a trade-off between the overall resistive power loss and the additional mass for the current collector material. However, in these devices, mechanical integrity is provided by the structural electrodes, allowing a range of collector designs to be considered. Using finite element simulations, these current collection strategies are explored quantitatively across a range of design space variables. The key conductivity parameters were measured experimentally, using the best existing materials, to inform direct current conduction simulations of the electrode/current collector assembly. For the present device configuration, the performance trade-off is governed by the area of the current collector. The most effective near-term strategy for power loss mitigation lies in reducing the contact resistance; however, improvements can also be obtained by modifying the collector geometry. The findings of this paper can be generalised to other structural power composites and monofunctional energy storage devices, which are relevant in many mass-sensitive electrochemical applications.

1. Introduction

Structural power composites (SPCs) [1–3] are an emerging class of multifunctional composite materials which can store and deliver electrochemical energy whilst bearing mechanical load. SPCs could be a key enabling technology for a range of applications, most notably in the electrification of transport, which is currently constrained by the relatively low specific energy of batteries [4]. By replacing conventional structural materials and energy storage devices with SPCs, dramatic reductions in the system mass and volume could be achieved [5]. Structural supercapacitor composites (SSC) are one class of SPCs that offer high power density, relevant to load-levelling and back-up power functions, combined with potentially long cycle life and environmental tolerance. This paper focuses [6] on carbon fibre/carbon aerogel (CF/CAG) structural electrodes [6], glass fibre structural separators, a bicontinuous structural electrolyte [7] and copper current collectors (Fig. 1). During the development of SPCs, little attention has been paid to the design of the current collectors (CCs), which draw electric current in/out of the electrochemical device. In conventional (monofunctional) devices, the CCs are continuous metallic foils which also act as supportive substrates upon which the active layer is deposited. However, this additional mass can be more than 14% of that of the total device [8]. In contrast, SSC electrodes are self-supporting, providing an opportunity to reduce the parasitic CC mass (and volume), by distributing additional metal only where it is needed. The carbon fibres generally used in SPCs provide a degree of multifunctional current collection, alongside their

* Corresponding author. Department of Aeronautics, Imperial College London, United Kingdom.
E-mail addresses: maria.valkova13@imperial.ac.uk (M. Valkova), snguyen@imperial.ac.uk (S. Nguyen), evgeny.senokos@mpikg.mpg.de (E. Senokos), s.razavi14@imperial.ac.uk (S. Razavi), anthony@imperial.ac.uk (A.R.J. Kucernak), d.anthony08@imperial.ac.uk (D.B. Anthony), m.shaffer@imperial.ac.uk (M.S.P. Shaffer), e.greenhalgh@imperial.ac.uk (E.S. Greenhalgh).

https://doi.org/10.1016/j.compscitech.2023.109978
Received 13 December 2022; Received in revised form 27 February 2023; Accepted 28 February 2023
Available online 4 March 2023

structural and electrochemical roles. It has often been tacitly assumed that no additional CC is needed, simply a contact at the device edge. In structural composite batteries, the assumption may be acceptable, at least for smaller, model devices. However, supercapacitors are intrinsically high power devices, and imply greater currents, requiring additional conductivity, particularly over larger devices/components. The common practice (Fig. 1) has been to use a narrow copper strip attached along one edge of each electrode as the CC [9]. However, since this configuration limits contact area and lengthens the path of charge carriers through the electrode, such a geometry may be detrimental to the delivered power [10], increasing the device equivalent series resistance (ESR). SSC devices have an area-normalised ESR (ca. 80 Ω cm^2 [6]) at least an order of magnitude higher than that of typical commercial monofunctional supercapacitors (ca. 3 Ω cm^2 [11]). Such a large ESR is a hurdle to scale-up, since charge collection inefficiencies increase with device area [12,13].

For conventional devices, as well as being highly electrically conductive, the current collector needs to be (electro)chemically compatible with the other device constituents and tolerate the manufacturing conditions. For structural power composites, there are the additional requirements since the device must carry significant (structural) mechanical loads. The current collector must, therefore, tolerate mechanical strain and adhere well to the electrodes and surrounding encapsulation such that it can provide efficient load-transfer across these interfaces. Design strategies for SPC current collectors that do not cover the entire structural electrode surface offer good opportunities for integration. However, the current collector materials must adhere well enough to facilitate infusion of liquid or structural electrolyte after assembly of the electrodes and separator.

Although copper CCs were selected for this modelling study, as they have been widely implemented in SPCs, the choice of CC material to use for structural power composites depends on the application requirements and the trade-offs between performance, cost and other considerations. For mass critical applications, the CC should be as light as possible, hence a high ratio of electrical conductivity to density may be preferred in future, for example, aluminium or nanocarbon based materials. The need for (electro)chemical compatibility places significant limitations, and different current collectors may be needed at the anode/cathode, particularly in battery or pseudocapacitive embodiments of SPC. If inherent passivation is not sufficient, deliberately engineered passivating coatings may be required. Finally, manufacturing considerations will be important, such as the ability to precisely deposit the CC in thin films that can conform well to the electrodes, potentially patterned according to the strategies discussed in this paper.

The design of current collectors in solar cells presents an analogous problem [14,15] but, in this context, area minimisation (i.e. shading losses) must be balanced with resistive losses [12]. Optimised metallic grids with parallel strips or 'busbar and fingers' designs [14] have been developed and analytical solutions for the minimum spacing [15] and width [14] of the grid elements based on the allowable losses have been derived. Current collector design to mitigate resistive losses is an active research area for many other electrochemical devices with low conductivity electrodes, such as fuel cells, electrolysers, and flow batteries, with both experimental [12,16] and computational [17–19] studies reported. The most important design factors are the quality of the electrode/CC interface [13,16] and the feature size of the CCs [17] but only simple geometries, such as parallel strips or regular grids, have been studied. Space-filling fractal grids [20] have the potential to enable more efficient current collection with a minimal amount of material. The fabrication of CCs with such complex architectures could use techniques such as screen printing [21].

The design of efficient CCs for structural supercapacitors could be explored through numerical direct current conduction models. Most computational analyses of resistive losses in electrochemical devices relate to the scalability of water splitting devices [17,18] using the two-dimensional (2D) models. However, such an approach would severely restrict the types of CC geometries that could be investigated. Given the influence of CC shape on the current distribution across the area of the cell, and considering the substantial thickness and anisotropic electrical conductivity of SSC electrodes [22], this system is more appropriately modelled as a three-dimensional (3D) domain. In addition, none of the prior studies consider CC mass (and volume), despite economic use of raw materials being an important driver.

This paper investigates the influence of CCs on the trade-off between resistive power losses and parasitic mass in structural supercapacitors, based on CF/CAG electrodes with copper CCs. By using a dimensionless design space diagram, the generalised current collection design problem has been considered and outline design strategies for various parameter regimes have been proposed. A 3D finite element model of direct current electrical conduction was used to evaluate the resistive power losses. To parametrise the model, the anisotropic electrode conductivity and contact conductivity of the electrode/current collector interface were characterised in four-probe resistance measurements. A series of parametric analyses were performed to evaluate the impact of active current density, cell surface area, CC area fraction, thickness, and shape. The data were used to generate Pareto fronts of optimum mass- and power-efficient CC solutions, and numerically evaluate their potential efficiency. Modifications to the electrode fabrication process are proposed to reduce contact resistance. The findings of this work may be applied to other SPCs, as well as conventional energy storage devices.

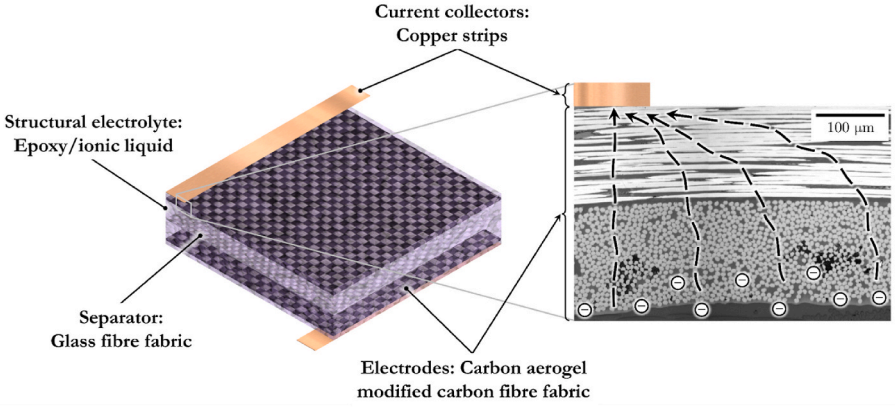

Fig. 1. Schematic of structural supercapacitor (SSC) device architecture (left), with partial cross-section illustrating electron paths from the electrode/electrolyte interface to the current collector (right).

2. Current collector design strategies for structural supercapacitors

The electrical resistance associated with current collection includes contributions from the electrode, the CC, and the contact interface between these two components. The design of efficient CCs, which co-minimise the total resistive power loss factor, P^*, and the current collector mass, m_{cc}, requires the designer to select appropriate values for the CC thickness, t_{cc}, its area fraction, A_f, (defined as $A_f = A_{cc}/A_{cell}$, where A_{cc} and A_{cell} are the geometric areas of the CC and the cell, respectively), and the bulk electrical conductivity of the CC material, σ_{cc}. The bulk electrical conductivity of the electrode, σ_e, the contact conductivity of the electrode/CC interface, σ_C, the current density, j_s, the length of the cell, L_{cell}, and its area, A_{cell}, will further impact the design. Taken together, these CC and cell variables form the design domain. Subsequent sections of this paper will interrogate this design space quantitatively through detailed modelling; however, the parameter regimes, which can be expected to produce efficient solutions, may also be identified by considering the basic principles of conduction.

The design domain can be simplified by introducing the non-dimensional variables σ_e/σ_{cc} and $\sigma_C L_{cell}/\sigma_e$. These ratios describe the relative importance of the resistive loss components in the system studied. For simplicity, this design domain analysis assumes an isotropic electrode conductivity and a square electrode geometry. It is also assumed that the density of the CC is greater than that of the electrode, as is typical for electrochemical cells. Further, the approach explores, at present, only solutions for CCs of constant thickness (as might be laid down with tape or patterned foil) and assumes a constant electrochemical current per unit area at peak current (a reasonable assumption if the electrode is homogeneous). Several regimes of interest were identified (Fig. 2).

In the theoretical limit $\sigma_e/\sigma_{cc} \geq 1$, assuming good contact between the electrode and the external circuit connections, no current collector is needed at all. In practice, the use of a current collector is necessitated by the limited conductivity of most electrode materials. In the limits $\sigma_e/\sigma_{cc} \to 0$ and/or $\sigma_C L_{cell}/\sigma_e \to 0$, a plate CC is necessary to minimise bulk electrode and contact losses, respectively. In such cases, mass reduction can only be achieved by reducing the CC thickness, as far as permitted by the CC conductivity and practical fabrication methods. For intermediate conductivity ratios, it is possible to optimise the CC area fraction and thickness by considering the tradeoff between CC mass and resistive losses. In the regime of low active current density, simple strip CC geometries (Fig. 2, green) may ensure resistive power losses remain low. The conductivity ratios of the specific system dictate the most appropriate design strategy. In the regime of high active current density, current collection is more demanding ($P^* \propto j_s$); therefore, more complex, grid current collector geometries (Fig. 2, blue) are advantageous. Large cell areas also increase the need for grid solutions ($P^* \propto A_{cell}$). At very low CC thicknesses, CC geometries with a hierarchical structure, which minimise losses within the CC grid elements may emerge as more efficient.

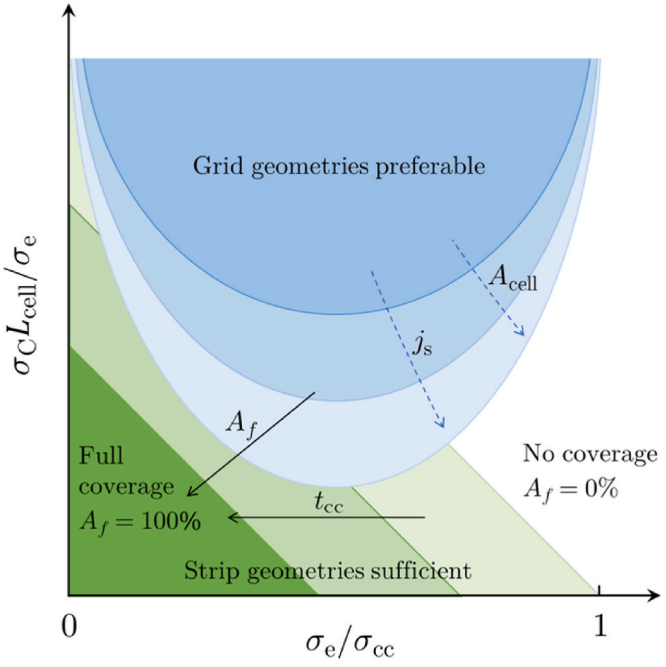

Fig. 2. Schematic representation of current collector design space, illustrating the parameter regimes where strip (green) or grid (blue) geometries are preferred. Solid arrows indicate recommended parameter selection; dash arrows indicate parameter influence over the size of the design regions.

3. Materials and characterisation methods

The as-received woven fabric was a 200 g/m^2 carbon fibre plain weave (C-WEAVE™ 200P 3K HS, Chomarat), containing Toray FT300B carbon fibres. The preparation of the CF/CAG electrodes and their application in structural supercapacitors are detailed elsewhere [6]. The electrode thickness (t_e) was 320 μm. The CC was a 10 mm wide copper tape with a one-sided conductive acrylic adhesive (AT526, Advance Tapes International), 35 μm foil thickness (t_{cc}). The copper tape was bonded to the as-produced electrode and cured inside a vacuum bag, at 1 bar and 130 °C held for 2 h. In this work, the above configuration is denoted '*Case I*'.

Additional studies focused on two potential fabrication strategies for improving the contact properties between the CAG-modified carbon fabric electrodes and the CC foils. The first strategy used selective masking of the CAG-modified fabric electrodes [23] to enable direct contact of the CC material to the carbon fibres ('*Case II*'). To model the potential improvement of this strategy, the contact and intrinsic conductivities of the carbon fabric which had been exposed to the same heating protocols as that used for the CAG synthesis, as described in Ref. [6], were characterised to provide the local material input parameters. The second strategy considered an electrically conductive surface treatment containing colloidal copper, which had shown promising results for Li-ion batteries [24] ('*Case III*'). The electrical design of cells involves co-optimisation of several resistive components [25]. In the case of SSC electrodes and CCs, this design requires knowledge of the conductivity of the electrode/current collector contact interface (σ_C) and the intrinsic conductivity of the electrode material (σ_e). However, the anisotropic electrical conductivity of the electrode necessitated characterisation along both the *lateral* ($\sigma_{e,x}$) and *transverse (i.e., through-thickness)* ($\sigma_{e,z}$) fabric directions (Fig. 3). Details of the measurements are in the ESI, whilst the results are in Table 1.

4. Finite element model

4.1. Geometry and boundary conditions

To understand the importance of electrical resistive losses in isolation, the analysis was restricted to the domain including a single electrode/CC assembly with a square device geometry (Fig. 3). The domain was modelled in 3D to account for the finite electrode thickness and material orthotropy, modeling the electrode as a continuous layer with homogenised properties. A uniform surface current density, j_s, acted over the electrode/separator interface plane, to represent the active current density. The separator was assumed to have negligible lateral conductivity. The effect of modifying the CC geometry could therefore be assessed by analysing the current distributions and heat dissipated within this domain. In most practical applications, several cells would be stacked, so the following design constraints were assumed: (i) uniform thickness of CCs, and (ii) external connection made through a single

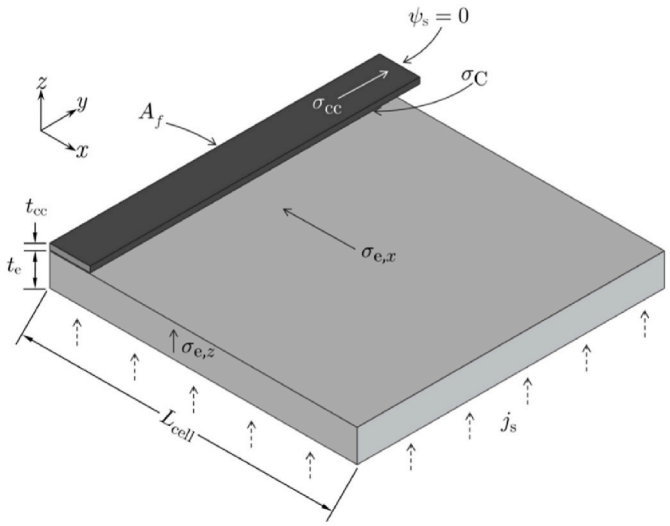

Fig. 3. Domain and boundary conditions for the current collection model (electrode in light grey, and current collector in dark grey).

Table 1
List of electric conductivities used in the three case studies.

Symbol	Quantity	Value			Unit
		Case I	Case II	Case III	
$\sigma_{e,x}$	Lateral conductivity of electrode	156	156	156	S/cm
$\sigma_{e,z}$	Transverse conductivity of electrode	0.17	0.15‡	0.17	S/cm
σ_{cc}	Conductivity of CC	5.95×10^5	5.95×10^5	5.95×10^5	S/cm
σ_C	Effective contact conductivity	0.95	3.58‡	14.45‡	S/cm^2

junction at the cell edge (referred to as the end-tab). An electrical ground was specified at the end-tab, whilst all other external surfaces were assumed to be electrically insulated. The geometric parameters of the assembly are listed in Table 2. In mass-insensitive applications, where CC design is only driven by minimising resistive loss, a planar sheet collector with full area coverage (Fig. 4e) is the optimal solution [26]. However, in mass-sensitive applications, where the CC mass and power losses must simultaneously be minimised, geometries with partial coverage can be advantageous. In this case, it is possible to co-optimise by modifying the geometric design of the CC.

Parametric studies considered a 'basic' set of geometries (Fig. 4), including a 'side-strip' (as used in existing devices), 'centre-strip', 'busbar and fingers', 'simple grid' and 'side-tabbed plate'. These parametric studies analysed the influence of: the CC area fraction (A_f), the CC thickness (t_{cc}), the active current density (j_s), the geometric side length of the cell (L_{cell}) and the contact conductivity (σ_C), with the range of values given in Table 2 (nominal values in bold). The nominal CC thickness (35 μm) was chosen to reflect the copper tape material, with

Table 2
List of geometric and cell parameters used in the current collection models.

Symbol	Quantity	Value	Unit
t_e	Electrode thickness	320	μm
t_{cc}	Current collector thickness	1, 2, 5,10, **35**	μm
L_{cell}	Cell length	0.9, **10**, 25	cm
A_f	Current collector area fraction	**10** … 100	%
j_s	Active current density	**1**, 10	mA/cm^2
V_R	Rated voltage	1	V

Nominal parameter values in bold.

lower thicknesses (down to 1 μm) investigated as potentially more efficient solutions: it should be noted that thicknesses lower than 5 μm require a change of application method. Nevertheless, these low thicknesses may be beneficial not only for reducing the parasitic CC mass, but also result in improved contact properties if conductive particles are able to ingress into the electrode surface. The electrical conductivities were assumed to be invariant with CC thickness, with the influence of the electrical conductivities investigated independently. The lengths were chosen to reflect device geometries which have been experimentally characterised [6]: equivalent to a 1 cm diameter coin cell (0.886 cm) and an A4 sheet (25 cm), whilst an intermediate value of 10 cm was also chosen which gave a straightforward numerical conversion between resistance and power loss. The active current density was kept constant for the different device sizes to permit performance comparisons (that is, scale-up analysis). The nominal active current density of $j_s = 1$ mA/cm^2 was representative of those used in experiments [6] and $j_s = 10$ mA/cm^2 (Section 5.1) was chosen to represent a more demanding electrical loading condition, such as constant voltage charging of demonstrator components [27]. The CC performance across all of the 'basic' geometries were compared under three contact configurations *Case I, II, and III*, representing different values of contact conductivity at the electrode/current collector interface.

An 'extended' set of geometries (ESI: Fig. S1) were also investigated, which included a selection of space-filling fractal grids [20]. Three grid densities were considered for each geometry. To minimise the number of simulations, this analysis only considered *Case III* (i.e., high contact conductivity), with the remaining parameters fixed at: $L_{cell} = 10$ cm, $j_s = 10$ mA/cm^2, $A_f = 10\%$, and $t_{cc} = 35$ μm.

4.2. Domain discretisation

The 3D nature of the problem and the anisotropic nature of the electrodes meant that the model was not tractable to a closed form analysis, and therefore finite element models for the detailed analysis of the CC performance were pursued. Using Abaqus [28], the geometries were discretised using solid quadratic (20-node) hexahedral thermal-electric elements (DC3D20E) to capture the potential gradients accurately. The meshes were structured using the volume partitioning technique to ensure a rectangular element shape and solved in a coupled thermal-electrical analysis. Mesh sensitivity studies were performed to ensure solution convergence and the numerical results were verified against 1D analytical solutions for the plate and side-strip geometries [23].

4.3. Constitutive model

Based on the electrode conductivity measurements (see ESI), orthotropic conductivity was assumed in the electrode domain whilst an isotropic material model was assumed in the CC domain. A surface-based contact interaction [28] was used to specify uniform contact conductivity at the electrode/current collector interface. For the baseline model (*Case I*), the contact conductivities measured for the CF/CAG and the cured copper CC were used. Additional case studies focused on the effects on CC performance of selective masking of the CF/CAG (*Case II*), and the use of an electrically conductive surface treatment (*Case III*). The measured and reported values of the contact conductivities were used to define the electrical contact. For *Case II*, the electrode conductivity in the regions underneath the contact zones were locally modified to reflect those measured on the heat-treated fabric. All constitutive parameters are in Table 1.

4.4. Performance evaluation

The methodology to evaluate the performance is detailed in the ESI, leading to the power loss coefficient being defined as $P^* = 2P_J/i_s V_R$

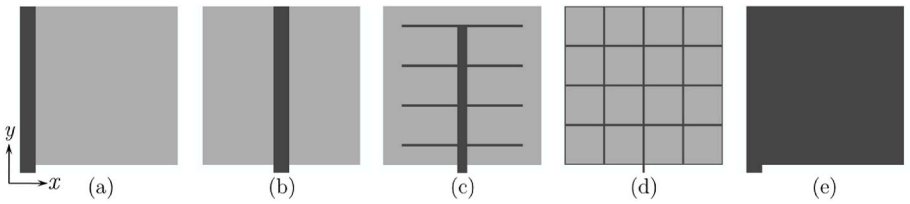

Fig. 4. 'Basic' set of current collector geometries investigated: (a) side-strip, (b) centre-strip, (c) busbar and 4 fingers and (d) simple 4x4 grid with A_f = 10%, and (e) side-tabbed plate with A_f = 100%.

where P_J was the total power dissipation due to resistive losses (Joule heating), i_s is the total active current and V_R is the rated voltage of the cell. The CC mass fraction was defined as $m_f = 2m_{cc}/m_{active}$, where m_{cc} is the mass of a single current collector and m_{active} is the mass of active materials in the cell: the two electrodes, separator, and electrolyte filling the pore space.

5. Results and discussion

5.1. Relative contributions to resistive loss and effect of current density

The power loss contributions due to the effective resistances of the electrode, CC, and the electrode/CC contact interface were calculated for the 'basic' geometries (Fig. 4). The corresponding power loss coefficients for the nominal model parameters are shown in Fig. 5(a). Contact resistance was the dominant source of power dissipation in all cases, and scaled inversely with the CC area fraction, leading to a contact power loss coefficient ca. 0.2% and ca. 2% for the full and partial (A_f = 10%) coverage current collector geometries, respectively. Amongst the partial coverage geometries, lateral resistive losses in the electrode varied significantly, decreasing by 98% between the 'side-strip' and 'simple grid' geometries. Total losses remained significantly lower for the 3.5 μm thick side-tabbed plate CC (referred to in the Figures as *side-tabbed plate'* to differentiate with the thicker embodiment) compared to all 35 μm thick 10% coverage geometries. The former solution therefore represents a more efficient material use, provided it is practical to use such a low thickness foil. When the current density was increased from 1 mA/cm^2 to 10 mA/cm^2 (Fig. 5(b)), the relative contributions of the loss components remained constant, and the power losses were directly proportional to the current density. At j_s = 10 mA/cm^2, contact resistance accounted for over 20% of the losses, illustrating the increasing importance of CC design at higher currents.

5.2. Effect of current collector area fraction and thickness

The power loss coefficient and mass fraction performance indices were calculated for the different partial coverage current collector geometries with A_f = 10%, across a range of area fractions and thicknesses (Fig. 6(a)). For a given CC thickness, reductions in power loss could be made by switching to a more efficient geometry, for example, from a side-strip to a busbar and fingers grid at t_{cc} = 35 μm. Fig. 6(a) also demonstrates that it is possible to achieve mass savings at no significant penalty to the power loss coefficient by reducing the CC thickness. For example, by switching from the 35 μm thick side strip to a 5 μm thick busbar and fingers grid, the CC mass can be reduced by 86% with a reduction in resistive power losses (compared to a 35 μm thick side strip). By considering a range of area fractions, in addition to thicknesses, Pareto fronts of optimal solutions (Fig. 6(b)) were constructed by selecting the minimum total power loss solution at each current collector thickness and area fraction.

5.3. Device scale-up

For a constant current density and CC area fraction, the power dissipation due to contact resistance was directly proportional to cell area: $P_{J,C} \propto A_{cell}$, since $R_C \propto 1/A_{cell}$ and $i_s \propto A_{cell}$. Based on initial analysis of the limiting case where current is collected from one cell edge, the lateral power dissipation in the electrodes and CC scales as $P_{J,e,l} \propto A_{cell}^2$ and $P_{J,cc} \propto A_{cell}^2$. In the limiting case where transverse current in the electrode is uniformly collected across its surface area, $P_{J,e,t} \propto A_{cell}$. For

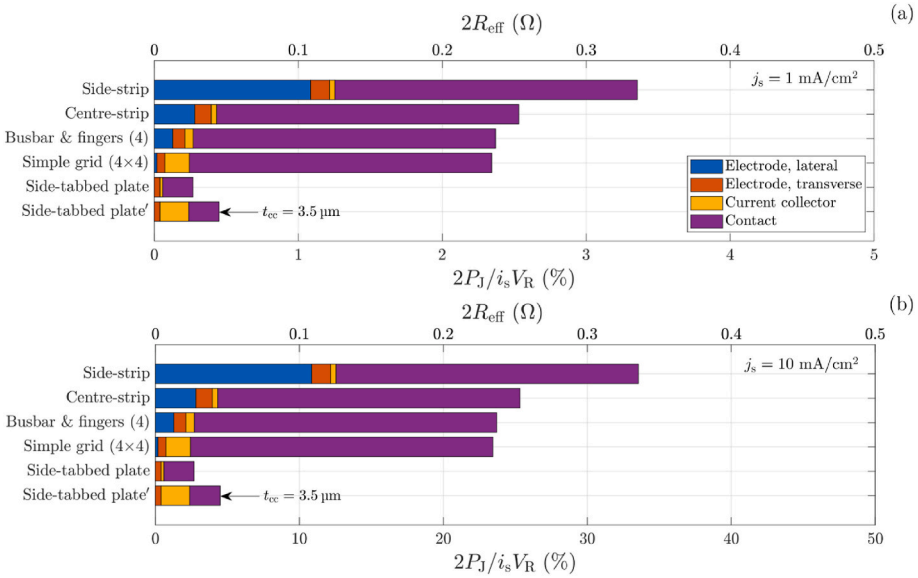

Fig. 5. Power loss coefficients for different partial coverage current collector geometries with A_f = 10% (with side-tabbed plate solutions shown for comparison) computed at (a) j_s = 1 mA/cm^2, and (b) j_s = 10 mA/cm^2. Case I, L_{cell} = 10 cm, t_{cc} = 35 μm unless otherwise indicated.

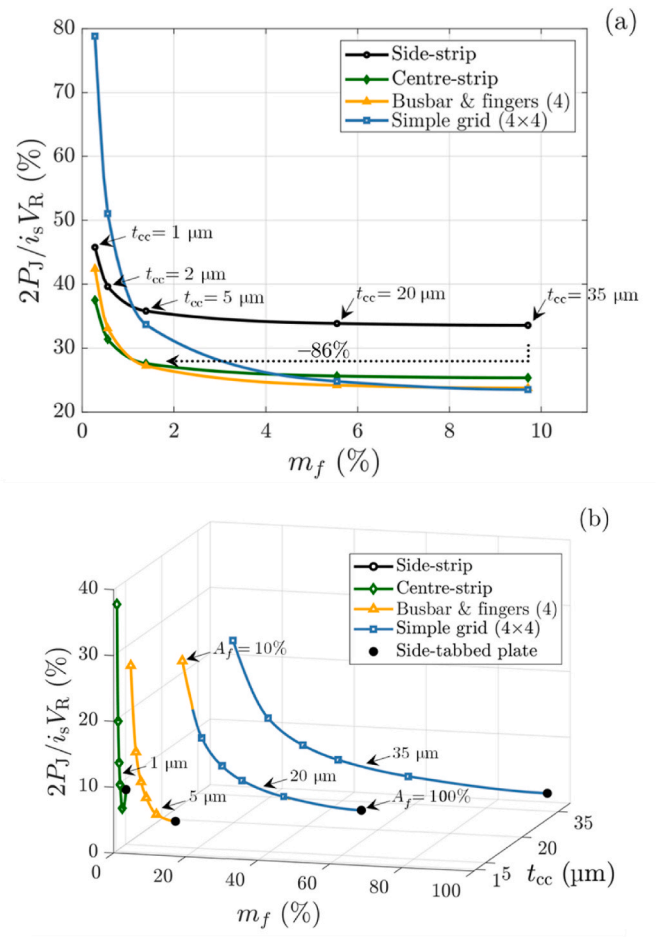

Fig. 6. (a) Total power loss coefficient and current collector mass fraction for partial coverage current collector geometries with $A_f = 10\%$, across a range of thicknesses. (b) Pareto frontiers across a range of current collector thicknesses. Case I, $j_s = 10$ mA/cm^2 and $L_{cell} = 10$ cm.

the partial CC geometries studied here, the proportionality was expected to be approximately linear for $P^*_{J,e,l}$ and $P^*_{J,cc}$, whilst $P^*_{J,e,t}$ and $P^*_{J,C}$ were expected to stay relatively constant with area.

The power losses and effective resistances for surface areas equivalent to those of a 1 cm diameter coin cell up to an equivalent A4 sized sheet using partial versus full coverage current collectors are plotted in Fig. 7(a) and (b), respectively. These results confirmed that the above relationships held for the electrode/CC assemblies. The relative increase in the power loss coefficient with cell area was more severe for CC geometries with less efficient lateral collection, such as the side strip collector (Fig. 7(a)), where lateral losses in the electrode outstripped contact losses for $A_{cell} > 200$ cm^2. Full coverage CCs did not accumulate lateral losses (Fig. 7(b)), and the slight increase in the power loss coefficient was due to power dissipation within the CC.

5.4. Effect of contact properties

As illustrated in Fig. 8, the contact resistance was inversely proportional to the contact conductivity. Therefore, the effect of modifying the contact conductivity was to change the importance of contact losses, relative to the other sources of resistive loss in the electrode/CC assembly. While contact losses could be reduced by ca. 74% through selective masking (*Case II*) [23], these contact losses still dominated the overall losses (at the nominal thickness) in all but the least efficient CC geometry (side-strip). Reducing contact losses by ca. 93% through using the colloidal copper surface treatment (*Case III*) depressed the contact losses to on par with that of the other sources of loss.

The 'extended' set of geometries (ESI: Fig. S2) was examined under *Case III* to understand the impact of the CC geometric design in the regime of low contact losses. However, the differences in overall power loss between the various grids were marginal. The busbar and finger design generally performed better than the simple or space-filling fractal grids. Whilst the simple and fractal grids generally had lower lateral electrode losses, this improvement was offset by higher CC losses. The latter were exacerbated as the grid density was increased due to the reduced width of grid elements (illustrated in Fig. 9(b) and (c)). The opposite was true for the lateral losses.

5.5. Design implications for structural supercapacitors

This work demonstrated that power performance of the present SSCs

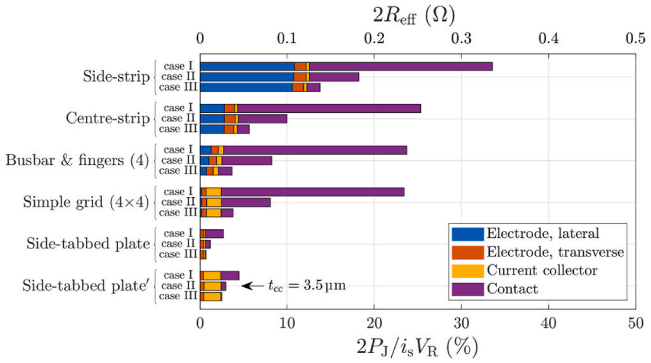

Fig. 8. Effect of contact properties on power loss coefficient and effective resistance. $L_{cell} = 10$ cm , $j_s = 10$ mA/cm^2 , $A_f = 10\%$, $t_{cc} = 35$ µm, unless otherwise indicated.

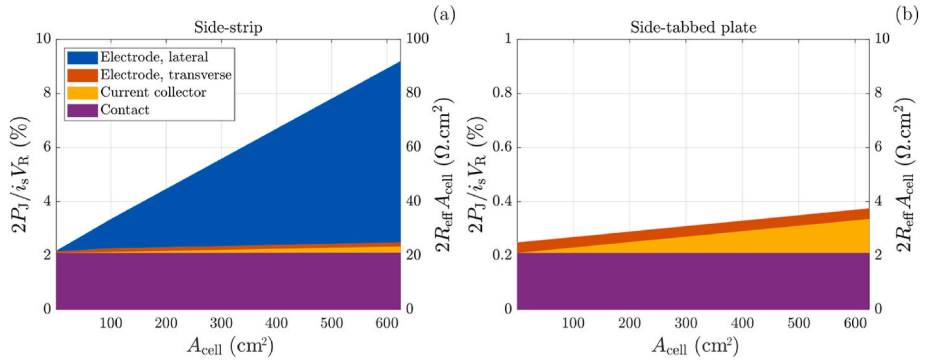

Fig. 7. Power loss coefficient and area-normalised resistance as a function of electrode surface area for: (a) side-strip with $A_f = 10\%$, and (b) side-tabbed plate current collector geometries. Case I, $L_{cell} = 0.9$, 10, 25 cm , $j_s = 1$ mA/cm^2 , $t_{cc} = 35$ µm.

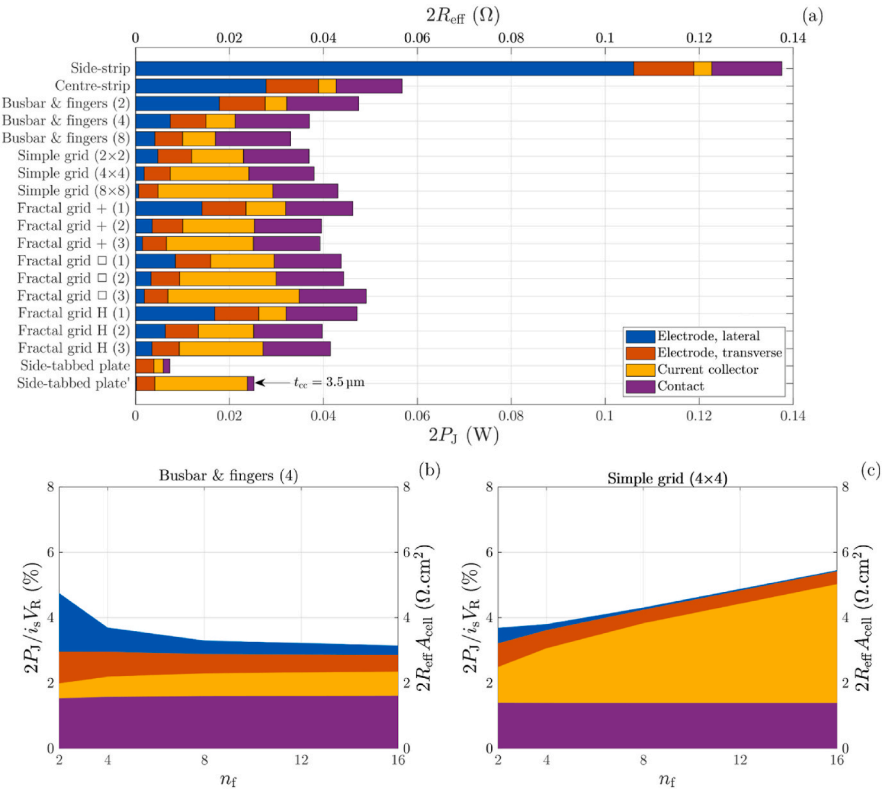

Fig. 9. (a) Power loss coefficient and effective resistance for partial coverage current collector geometries (with side-tabbed plate for comparison); and effect of grid density (number of fingers n_f) on power loss contributions in (b) busbar and fingers, and (c) simple grid current collectors. Case III, $L_{cell} = 10$ cm ,$j_s = 10$ mA/cm^2 ,$A_f = 10\%, t_{cc} = 35$ μm.

is limited chiefly by the poor contact conductivity of the electrode/CC interface, and somewhat by the lateral electrode conductivity (Fig. 5). Therefore, the most effective route to minimise resistive power losses is to maximise the CC area fraction (Fig. 2, green region). To ensure parasitic mass is kept low, the foil thickness should be simultaneously reduced. The numerical results suggest that resistive losses would remain acceptably low for 1 μm foil thicknesses. However, practical considerations, such as durability and scalability, may prevent the use of ultra-thin foils. For the present SSCs [6], post-infusion of the electrodes with ionic liquid is required and so full coverage CCs are unsuitable. In this case, geometries with partial area fractions can offer a good compromise between mass and power losses, provided they are appropriately designed.

These findings challenge the prevailing design strategies for CC in reported SPC embodiments [1,2], demonstrating that the widely used side-strip collectors are an inefficient solution, due to high lateral losses in the electrode (Fig. 5). For a 10% CC area fraction, these losses could be reduced by 98% by replacing the side-strip with the simple grid, which can be attributed to the reduced lateral current path. This reduction is slightly offset by an increase in CC resistance in the narrower grid elements. This width is particularly important where the current is largest, such as near end tabs.

To obtain a simultaneous reduction in the CC mass, alternative designs with hierarchical structures are advantageous. Fig. 6(a) shows that, with a busbar and fingers design, which is wider near the end tab, thicknesses as low as 5 μm could be used (a CC mass reduction of 86% compared to that for the nominal thickness) without significantly increasing overall power loss. This analysis explains why the Pareto fronts (Fig. 6(b)) show that as the thickness reduces, the minimum power loss solutions transition from the 'simple grid' to 'busbar and fingers', to 'centre-strip' geometries, eventually collapsing to the plate solution. Section 5.4 demonstrated how the design problem changes if contact resistance ceases to be the dominant source of loss. When dense grids were considered, the fractal grids were not advantageous over busbar and fingers grids.

The busbar and fingers class of geometries are, therefore, considered the ideal candidate for future SSC CCs, and future work should aim to reduce the foil thickness. Grid elements with a tapered geometry or variable thickness could be also explored, perhaps using new fabrication routes. The choice of route should consider material cost and sustainability, as well as the material adhesive properties, conductivity and compatibility with the electrolyte. It should be noted that improved conformal contact should inherently be enhanced through adopting printing techniques.

5.6. *Model limitations and remaining research questions*

The present model assumes a uniform electrode geometry and uniform active current density applied at the electrode/electrolyte plane. The model assumed a simple transversely isotropic material model for the electrodes, which was parametrised using the effective lateral conductivity measured from 0°/90° fabric specimens. Despite these simplifications, the numerical results represent a useful initial estimate of resistive losses in the electrode/current collector assembly, and deviations from the assumed behaviour are expected to be low. Future work could improve the model by employing either (a) a constitutive model that has a fibre orientation-dependent conductivity, or (b) a mesoscale geometric fabric model. The latter would be more challenging because it would require constitutive data to be measured for single yarns and their interfaces.

To validate the models, experiments should be conducted on full devices (containing the same constituents modelled with either a liquid or structural electrolyte) using a selection of current collector geometries that encompasses the most important geometries studied, as shown in Fig. 4. Although the models did not include an electrolyte, the electrolyte would be necessary to characterise the electrochemical

performance with various current collectors. Electrochemical impedance spectroscopy [6] and equivalent circuit analyses would be used to determine the resistances associated with the current collection and the electrolyte. The main comparison between the models and the experimental results would focus on the effect of the current collection architecture on the power losses associated only with the current collection.

Finally, it should be noted that this study has not considered the durability and mechanical aspects of the current collection. In particular, making the current collector very thin may lead to durability and bonding issues, particularly under cyclic loading. Furthermore, the current collector needs to provide good mechanical load transfer across the electrode/current collector/encapsulation interface. This interaction is vital to realise the mechanical contribution of the structural power device to the overall system.

6. Concluding remarks

Structural supercapacitors must provide high gravimetric electrical and mechanical properties; however, their scale-up to real applications (i.e., m^2) is limited by high internal resistance and the CC mass, where the aspiration is to deliver multifunctional components fabricated from large cells with minimal joints/interfaces between them. Considering the vital role of CCs, new design strategies have been sought to maximise power- and mass-efficiency by considering the CC design. A generalised design space analysis was presented and strategies for lightweight and power-efficient CCs for different regimes were outlined. 3D direct current conduction simulations for quantitative evaluation of CC performance in structural supercapacitors based on CF/CAG and copper CCs was then undertaken.

High contact resistance was the principal performance limiting factor for CCs in existing structural supercapacitors, and therefore the most effective near-term strategies for mitigation of the losses lies in improving contact conductivity, increasing the area fraction and reducing the foil thickness. This strategy challenges the prevailing 'side-strip' CC design, which is associated with large lateral losses in the electrode and could be reduced by 98% by using a 'simple grid' CC. Significant mass reductions of 86% could be obtained by using thin 'busbar and fingers' CCs. The benefits of CC grids with greater width near the end tabs increase with current densities and device areas.

Though formal optimisation of individual CC geometries was outside the scope, future work will focus on optimising geometries of interest. Future work is also planned to exploit the findings through manufacture of the proposed CC grids reported here.

The trade-off analysis methodology presented here can be applied to other SPCs, such as structural batteries, and is relevant to many mass-sensitive energy storage applications. The present numerical model is readily applicable to a wide range of electrode chemistries, as well as non-metallic or anisotropic CCs. In future, analysis could consider additional relevant performance characteristics, such as cost and sustainability to better inform current collector material choice and design.

CRediT author statement

Maria Valkova: Conceptualization, Validation, Formal Analysis, Investigation, Data Curation, Writing - Original Draft, Writing - Review & Editing, Visualization. **Sang Nguyen:** Conceptualization, Validation, Formal Analysis, Investigation, Data Curation, Writing - Original Draft, Writing - Review & Editing, Visualization. **Evgeny Senokos:** Investigation, Writing - Review & Editing. **Seyedalireza Razavi:** Investigation, Writing - Review & Editing. **Anthony Kucernak:** Writing - Review & Editing. **David Anthony:** Investigation, Writing - Review & Editing. **Milo Shaffer:** Formal Analysis, Investigation, Writing - Review & Editing. **Emile S Greenhalgh:** Conceptualization, Methodology, Data Curation, Writing - Original Draft, Funding acquisition.

Declaration of competing interest

The authors declare that they have no known competing financial interests or personal relationships that could have appeared to influence the work reported in this paper.

Data availability

Data will be made available on request.

Acknowledgements

This work has been funded by the EPSRC Future Composites Research Manufacturing Hub (EP/P006701/1), the EPSRC Beyond Structural project (EP/P007465/1), the European Office of Aerospace Research and Development (IOE Grant FA9550-17-1-0251) and EU Clean Sky 2 (SORCERER Project #738085). This research was supported by the Royal Academy of Engineering under the Chairs in Emerging Technologies scheme. The authors gratefully acknowledge Chomarat for supplying the materials and Colleen Jackson for help with resistance measurements. For the purpose of open access, the author has applied a Creative Commons Attribution (CC BY) licence to any Author Accepted Manuscript version arising.

Appendix A. Supplementary data

Supplementary data to this article can be found online at https://doi.org/10.1016/j.compscitech.2023.109978.

References

[1] Y. Xu, W. Lu, G. Xu, T.-W.W. Chou, Structural supercapacitor composites: a review, Compos. Sci. Technol. 204 (2021), 108636.
[2] L.E. Asp, M. Johansson, G. Lindbergh, J. Xu, D. Zenkert, Structural battery composites: a review, Funct. Compos. Struct. 1 (2019), 42001.
[3] E.S. Greenhalgh, S. Nguyen, M. Valkova, N. Shirshova, M.S.P. Shaffer, A.R. J. Kucernak, A critical review of structural supercapacitors and outlook on future research challenges, Compos. Sci. Technol. 235 (2023), 109968.
[4] A.W. Schäfer, S.R.H. Barrett, K. Doyme, L.M. Dray, A.R. Gnadt, R. Self, A. O'Sullivan, A.P. Synodinos, A.J. Torija, Technological, economic and environmental prospects of all-electric aircraft, Nat. Energy 4 (2019) 160–166.
[5] S.N. Nguyen, A. Millereux, A. Pouyat, E.S. Greenhalgh, M.S.P. Shaffer, A.R. J. Kucernak, P. Linde, Conceptual multifunctional design, feasibility and requirements for structural power in aircraft cabins, J. Aircraft 58 (2021) 677–687.
[6] M.F. Pernice, G. Qi, E. Senokos, D.B. Anthony, S. Nguyen, M. Valkova, E. S. Greenhalgh, M.S.P. Shaffer, A.R.J. Kucernak, Mechanical, electrochemical and multifunctional performance of a CFRP/carbon aerogel structural supercapacitor and its corresponding monofunctional equivalents, Multifunct. Mater. 5 (2022), 025002.
[7] Q. Wendong, J. Dent, V. Arrighi, L. Cavalcanti, M.S.P. Shaffer, N. Shirshova, Biphasic epoxy-ionic liquid structural electrolytes : minimising feature size through cure cycle and multifunctional block-copolymer addition, Multifunct. Mater. 4 (2021), 035003.
[8] M.A. Cusenza, S. Bobba, F. Ardente, M. Cellura, F. Di Persio, Energy and environmental assessment of a traction lithium-ion battery pack for plug-in hybrid electric vehicles, J. Clean. Prod. 215 (2019) 634–649.
[9] E.S. Greenhalgh, J. Ankersen, L.E. Asp, A. Bismarck, Q.P.V. Fontana, M. Houlle, G. Kalinka, A.R.J. Kucernak, M. Mistry, S. Nguyen, H. Qian, M.S.P. Shaffer, N. Shirshova, J.H.G. Steinke, M. Wienrich, Mechanical, electrical and microstructural characterisation of multifunctional structural power composites, J. Compos. Mater. 49 (2015) 1823–1834.
[10] B.K. Kim, S. Sy, A. Yu, J. Zhang, Electrochemical supercapacitors for energy storage and conversion, in: Handb. Clean Energy Syst., 2015, pp. 1–25.
[11] Maxwell Technologies, Datasheet: 2, 7V 100F Ultracapacitor Cell, 2018.
[12] A.I. Pereira, J. Martins, C.J. Tavares, L. Andrade, A. Mendes, Development of stable current collectors for large area dye-sensitized solar cells, Appl. Surf. Sci. 423 (2017) 549–556.
[13] P. Tammela, H. Olsson, M. Strømme, L. Nyholm, The influence of electrode and separator thickness on the cell resistance of symmetric cellulose-polypyrrole-based electric energy storage devices, J. Power Sources 272 (2014) 468–475.
[14] H.B. Serreze, Optimizing solar cell performance by simultaneous consideration of grid pattern design and interconnect configuration, Conf. Rec. IEEE Photovolt. Spec. Conf. (1978) 609–614.
[15] J.R. Hauser, P.M. Dunbar, Performance limitations of silicon solar cells, IEEE Trans. Electron. Dev. (1977) 305–321. ED-24.

[16] H.S. Noh, J. Hwang, K. Yoon, B.K. Kim, H.W. Lee, J.H. Lee, J.W. Son, Optimization of current collection to reduce the lateral conduction loss of thin-film-processed cathodes, J. Power Sources 230 (2013) 109–114.
[17] F.F. Abdi, R.R. Gutierrez Perez, S. Haussener, Mitigating voltage losses in photoelectrochemical cell scale-up, Sustain. Energy Fuels 4 (2020) 2734–2740.
[18] A. Hankin, F.E. Bedoya-Lora, C.K. Ong, J.C. Alexander, F. Petter, G.H. Kelsall, From millimetres to metres: the critical role of current density distributions in photo-electrochemical reactor design, Energy Environ. Sci. 10 (2017) 346–360.
[19] Y. Kamenev, A. Kiselevich, E. Ostapenko, Evaluation of criteria for design of current collectors of the lead-acid battery, J. Power Sources 110 (2002) 133–137.
[20] D. Hurst, J.C. Vassilicos, Scalings and decay of fractal-generated turbulence, Phys. Fluids 19 (2007).
[21] W. Johannisson, D. Carlstedt, A. Nasiri, C. Buggisch, P. Linde, D. Zenkert, L.E. Asp, G. Lindbergh, B. Fiedler, A screen-printing method for manufacturing of current collectors for structural batteries, Multifunct. Mater. 4 (2021), 035002.
[22] S. Nguyen, D.B. Anthony, H. Qian, C. Yue, A. Singh, A. Bismarck, M.S.P. Shaffer, E. S. Greenhalgh, Mechanical and physical performance of carbon aerogel reinforced carbon fibre hierarchical composites, Compos. Sci. Technol. 182 (2019), 107720.
[23] M.I. Valkova, Characterising, Understanding and Predicting the Performance of Structural Power Composites, Imperial College London, 2022.
[24] P. Taheri, S. Hsieh, M. Bahrami, Investigating electrical contact resistance losses in lithium-ion battery assemblies for hybrid and electric vehicles, J. Power Sources 196 (2011) 6525–6533.
[25] R. Janoch, A.M. Gabor, A. Anselmo, C.E. Dube, Contact resistance measurement - observations on technique and test parameters, in: 2015 IEEE 42nd Photovolt. Spec. Conf. PVSC 2015, New Orleans, 2015, pp. 1–6.
[26] P. Tan, L. Tong, G.P. Steven, Micromechanics models for the elastic constants and failure strengths of plain weave composites, Compos. Struct. (1999) 797–804.
[27] S.N. Nguyen, D.B. Anthony, T.J. Katafiasz, G. Qi, S. Razavi, E. Senokos, E. S. Greenhalgh, M.S.P. Shaffer, A.R.J. Kucernak, P. Linde, Manufacture and characterisation of a structural supercapacitor demonstrator, Compos. Sci. Technol. (2023) (submitted for publication).
[28] Dassault Systèmes Simulia, Abaqus Analysis User's Manual, 2012.